physical causation of the excess rainfall comes from ensemble integrations of the uncoupled atmosphere model forced by observed SST, which also produce a strong wet signal over Europe for summer 1997.

The ensemble mean precipitation anomalies forecast for December 1997 to February 1998 are shown in Fig. 3b. These forecasts start in September and October, and in all cases the predicted SST shows El Niño conditions at least as strong as 1982–83 during northern winter. The plot shows an even stronger level of signal than summer 1997, and the general pattern of the precipitation anomalies is very plausible for a strong El Niño event. We note, for example, the wet signal in California, Florida, Uruguay and East Africa, and the dry signal in the Amazon region and southern Africa. More interesting are those features which might not have been expected empirically, but have apparently occurred: wet conditions in India and southeast China, a lack of drought in northern Australia, and wet weather in western Europe. Figure 3c shows our latest forecast, for the period March–May 1998. The model rainfall distribution is again significantly shifted in many regions of the world.

Empirical studies show evidence of links between some aspects of European weather and El Niño and other factors, but correlations are relatively low[2,17] and an El Niño signal tends to be visible only in winter months. As far as we know, no empirical scheme would have predicted the summer 1997 European rainfall from the data available in April. One should not draw too much from a single case, but it seems that at least in some instances a model-based approach goes beyond what present-day empiricism can do.

It is our belief that dynamical methods offer the best long-term hope for making seasonal forecasts because of their greater generality and precision: that is, because of their ability to handle unprecedented situations and to treat nonlinear combinations of factors which cannot be extracted empirically from the short observational records available to us. Dynamical models still have relatively large errors, and cannot yet be considered reliable. Nonetheless, our results suggest that useful model-based seasonal forecasting is now possible. Future improvements in models and their initialization can only increase the reliability and usefulness of such forecasts in the years to come. □

Received 21 August 1997; accepted 25 February 1998.

1. Palmer, T. N. Extended range atmospheric prediction and the Lorenz model. *Bull. Am. Meteorol. Soc.* **74,** 49–65 (1993).
2. Barnston, A. G. Linear statistical short-term climate predictive skill in the northern hemisphere. *J. Clim.* **7,** 1513–1564 (1994).
3. Barnett, T. P. *et al.* Forecasting global ENSO-related climate anomalies. *Tellus A* **46,** 367–380 (1994).
4. Livezey, R. E., Masutani, M. & Ji, M. SST-forced seasonal simulation and prediction skill for versions of the NCEP/MRF model. *Bull. Am. Meteorol. Soc.* **77,** 507–517 (1996).
5. Ji, M., Leetmaa, A. & Kousky, V. E. Coupled model predictions of ENSO during the 1980s and the 1990s at the National Centers for Environmental Prediction. *J. Clim.* **9,** 3105–3120 (1996).
6. Palmer, T. N. & Anderson, D. L. T. The prospects for seasonal forecasting: a review. *Q. J. R. Meteorol. Soc.* **120,** 755–793 (1995).
7. Hastenrath, S. Recent advances in tropical climate prediction. *J. Clim.* **8,** 1519–1532 (1995).
8. Livezey, R. E. *et al.* Teleconnective response of the Pacific-North American region atmosphere to large central Pacific SST anomalies. *J. Clim.* **10,** 1787–1820 (1997).
9. Reynolds, R. W. & Smith, T. M. Improved global sea surface temperature analyses using optimum interpolation. *J. Clim.* **7,** 929–948 (1994).
10. Smith, N., Blomley, J. E. & Meyers, G. A univariate statistical interpolation scheme for subsurface thermal analyses in the tropical oceans. *Prog. Oceanogr.* **28,** 219–256 (1991).
11. Stockdale, T. N. Coupled ocean-atmosphere forecasts in the presence of climate drift. *Mon. Weath. Rev.* **125,** 809–818 (1997).
12. Blanke, B., Neelin, J. D. & Gutzler, D. Estimating the effect of stochastic wind stress forcing on ENSO irregularity. *J. Clim.* **10,** 1473–1486 (1997).
13. Eckert, C. & Latif, M. Predictability of a stochastically forced hybrid coupled model of El Niño. *J. Clim.* **10,** 1488–1504 (1997).
14. Kleeman, R. & Moore, A. M. A theory for the limitationof ENSO predictability due to stochastic atmospheric transients. *J. Atmos. Sci.* **54,** 753–767 (1997).
15. Stockdale, T., Latif, M., Burgers, G. & Wolff, J.-O. Some sensitivities of a coupled ocean-atmosphere GCM. *Tellus A* **46,** 367–380 (1994).
16. Wonnacott, T. H. & Wonnacott, R. J. *Introductory Statistics* (Wiley, New York, 1977).
17. Fraedrich, K. An ENSO impact on Europe? A review. *Tellus A* **46,** 541–552 (1994).

Acknowledgements. The model integrations were carried out on a VPP300 machine donated by Fujitsu Limited. The ocean model was provided by the Max-Planck-Institut für Meteorologie, Hamburg; ocean data assimilation software by the Bureau of Meteorology Research Centre, Melbourne; and coupling software by CERFACS, Toulouse.

Correspondence and requests for materials should be addressed to T.N.S. (e-mail: t.stockdale@ecmwf.int). Further information and forecast plots can be found on the ECMWF Seasonal Forecast Project Web pages at http://www.ecmwf.int

Ice-sheet variability around the North Atlantic Ocean during the last deglaciation

A. Marshall McCabe* & Peter U. Clark†

** School of Environmental Studies, University of Ulster, Coleraine, County Londonderry, Northern Ireland BT52 1SA, UK*

† Department of Geosciences, Oregon State University, Corvallis, Oregon 97331, USA

Millennial-scale variability in the flux of ice-rafted detritus to North Atlantic sediments during the last glacial period has been interpreted to reflect a climate-forced increase in the discharge of icebergs from ice-sheet margins surrounding the northern North Atlantic Ocean[1]. But the relationship between ice-sheet variability and climate change is not clear, as both the sources of ice-rafted detritus and the ice-marginal processes are varied and complex[2–4]. Terrestrial records are helpful in unravelling this complexity because they can demonstrate the scale of ice-sheet oscillations, and whether the ice sheet (or sector) was advancing or retreating with respect to climate change. Here we constrain the age and anatomy of a prominent readvance of the British Ice Sheet in the northern Irish Sea region at ~14 ^{14}C kyr BP (~16.4 calendar kyr BP). The analysis indicates that the British Ice Sheet participated in an iceberg discharge episode known as Heinrich event 1. Comparison with other terrestrial and marine ice-sheet records suggests that the dynamic collapse of the Laurentide Ice Sheet beginning at 14.6–15.0 ^{14}C kyr BP[1,4] (~17.2–17.6 calendar kyr BP)[5] initiated varied responses from other ice-sheet margins around the northern North Atlantic region. These observations support the argument that the release of icebergs and meltwater during Heinrich event 1 disrupted the North Atlantic thermohaline circulation[6–8], leading to a delay or reversal of deglaciation of the Northern Hemisphere and at least as far south as 40° S for two to three thousand years[5,9,10], suggesting a climate forcing and response similar to that of the ensuing Younger Dryas 'cold snap'[11,12].

Terrestrial records of millennial-scale ice-sheet oscillations should be present in the climatically sensitive northeastern Atlantic region, but they have a low preservation potential along continental margins, reflecting the duration and erosional effects of ice cover on the continental shelf. However, geological records of oscillations of the Irish Sea basin ice stream, which was a major conduit for British Ice Sheet (BIS) drainage during the last deglaciation (Fig. 1), are well preserved because they offlap northwards (inland) towards centres of ice dispersion. This ice stream experienced at least five ice-marginal oscillations between 22 and 14 ^{14}C kyr BP[13], suggesting similar millennial-scale variability as identified for other amphi-North Atlantic ice sheets. The phasing relations between BIS variability and that of other ice sheets, however, has not been rigorously established.

On the northwestern margins of the Irish Sea basin, the outer limit (130 km long) of a major southeasterly ice readvance from the Irish lowlands is marked by a narrow (1–3 km) terminal zone of ice-contact landforms (Fig. 1). On the margins of Dundalk Bay and Carlingford Lough, moraines and deltas overlie interstadial muds and mark the former extent of grounded ice lobes that ended in shallow marine settings. To the northeast at Killard Point, the same ice limit is marked by a raised ice-contact morainal bank which prograded southeastwards into the sea. The bank is dominated by boulder gravel and marine mud within multistoried channels which record a high sediment flux to the ice margin. The presence of raised, late-glacial shoreface gravels immediately beyond these limits indicates synchroneity between ice lobe maxima and high relative sea level.

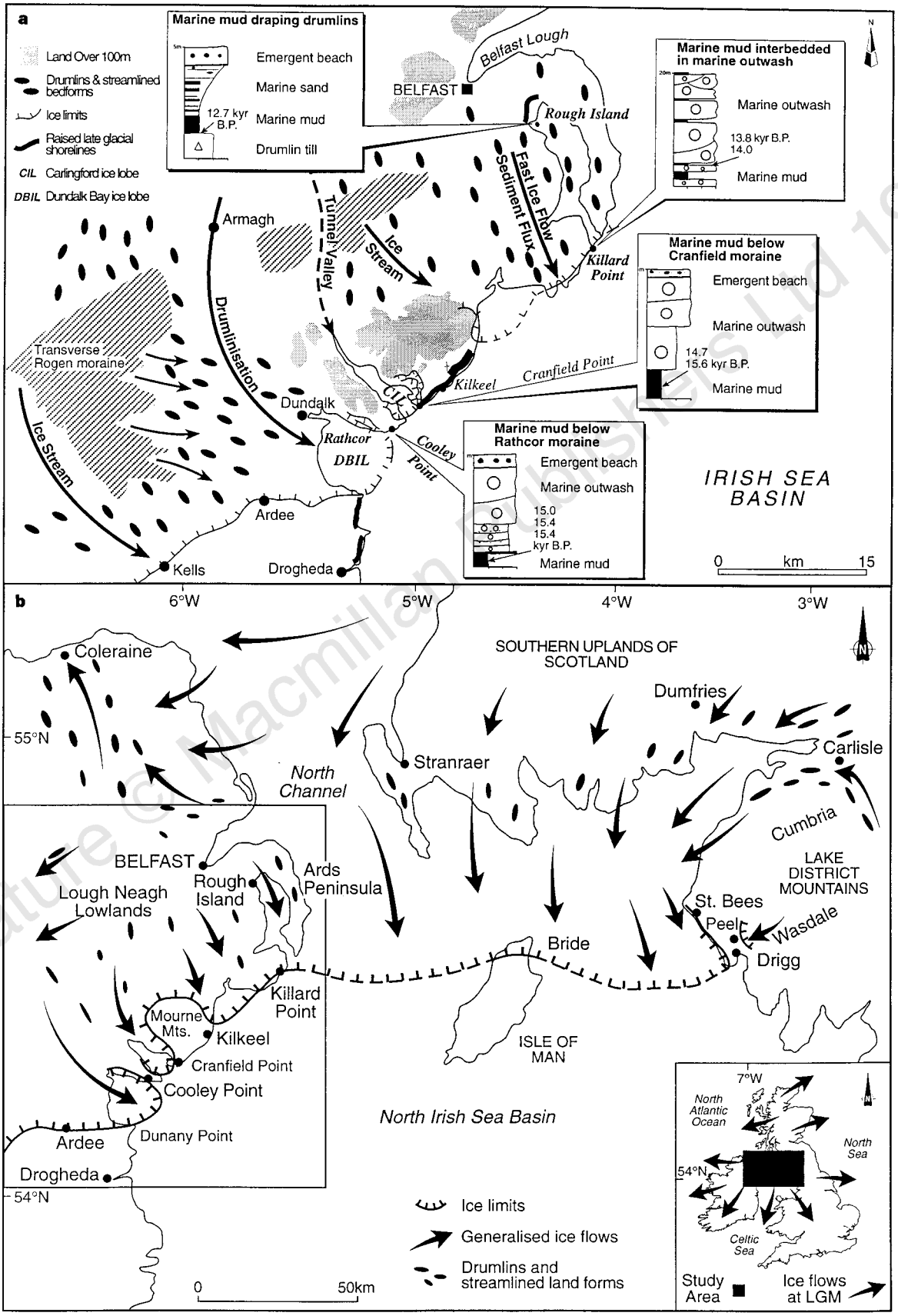

Figure 1 a, Deglacial records in the north Irish Sea basin. Pattern of ice flow during H1 and the stratigraphic position of dated marine mud beds in the north Irish Sea basin. **b**, Ice flows and H1 ice limits in the north Irish Sea basin. Inset, ice flows in Britain during the LGM.

Drumlins occur within 1–6 km up ice of the terminal moraines. Ice flow lines identified from these bedforms indicate contemporaneity of drumlinization (fast ice flow) and moraine building. Inland from Dundalk, drumlinization along a curved flow path crosscuts and overprints a prominent zone of Rogen moraine ridges, suggesting that bed reorganization and sediment transfer to ice margins occurred during ice readvance (Fig. 1). The belt of pristine Rogen moraine 25 km inland from Dundalk suggests that the ice sheet had only retreated a short distance before drumlinization and ice readvance. The presence of a regional drape of red marine mud directly overlying drumlin tills in the Ards Peninsula, and the absence of fluvioglacial deposits inland of the moraines, indicates that drumlinization was followed closely by rapid ice retreat.

On the northern margins of the Irish Sea basin, regional ice flow lines reconstructed from drumlins are also bounded by limiting moraines on the Isle of Man (Bride) and along the Cumbrian coast (St Bees, Drigg). The pattern of ice flow associated with these moraines is similar to the readvance across eastern Ireland and suggests a regional pattern of convergent ice flow from separate ice centres into the northern Irish Sea basin at this time (Fig. 1).

The age of this readvance is constrained by accelerator mass spectrometry ^{14}C dating of the benthonic foraminifera *Elphidium clavatum* sampled from marine muds below and interbedded with ice-contact outwash at four sites along the ice limit (Fig. 1 and Table 1). Microfaunas in these mud beds are dominated by *E. clavatum* (85–95%) and the ostracod *Roundstonia globulifera* (5–10%) which shows intact instars. Similar opportunistic biocoenoses have been recorded from contemporary Arctic–subarctic areas recently vacated by tidewater glaciers, and are typical of glaciomarine environments (0.5–2.5 °C, turbid, lowered salinities)[14]. The AMS ^{14}C dates (Table 1) and lithostratigraphy (Fig. 1) provide a coherent time frame for palaeoenvironmental changes occurring before, during and after the readvance in the north Irish Sea basin (Cooley Point interstadial, from ≥16.7 and ≤14.7 ^{14}C kyr BP; Killard Point stadial, with ice margin advance after 14.7 ^{14}C kyr BP and at its maximum position at 14.0 ^{14}C kyr BP; Rough Island interstadial with rapid retreat after 13.8 ^{14}C kyr BP). Our results from these terrestrial records thus show that rapid ice accumulation and advance in the northern sectors of the BIS occurred during Heinrich event 1 (H1) following early widespread deglaciation along the southern part of the ice sheet between ≥16.7 and ≤14.7 ^{14}C kyr BP. The Killard Point Stadial therefore documents a major deglacial oscillation of the BIS preceding the Loch Lomond stadial, which is marked by renewed ice-sheet development in the highlands of western Scotland during the Younger Dryas[15] (10–11 ^{14}C kyr BP).

The new data from the Irish Sea basin provide critical new information for comparing ice-marginal events in the amphi-North Atlantic during H1. In Fig. 2, we compare terrestrial and marine records which demonstrate that several sectors of several ice sheets around the North Atlantic advanced during H1, whereas other ice sheets began to retreat at or shortly following the beginning of H1. Ice-rafted detritus (IRD) records suggest synchronous increases in the flux of icebergs delivered from ice streams draining the Laurentide Ice Sheet (LIS) through Hudson Strait and the Gulf of St Lawrence beginning 14.6 to 15 ^{14}C kyr BP[1,4] (Fig. 2d). Records from the southern margin of the LIS suggest that, following a major retreat that ended at 15.0–15.5 ^{14}C kyr BP (Erie interstade), the margin readvanced (Port Bruce stade, Crown Point phase) several hundred kilometres to within <150 km of its maximum Late Wisconsin position and then retreated rapidly during or near the end of H1 (refs 16, 17; Fig. 2e). Our data from the northern Irish Sea area suggest a similar sequence of events for the BIS, with an interstadial preceding a readvance of the ice margin which was at its maximum position at 14 ^{14}C kyr BP, and was followed by rapid retreat after 13.8 ^{14}C kyr BP (Fig. 2c). We do not know precisely when the BIS began to readvance, but out data suggest that it was at its maximum position at a time (13.8–14 ^{14}C kyr BP) when retreat of the southern margin of the LIS was well underway (Fig. 2e). Bond and Lotti[1] argue from IRD data that the Icelandic Ice Sheet (IIS) began to discharge icebergs at the same time as marine ice streams that drained the LIS. The eastern Greenland Ice Sheet (GIS) began to

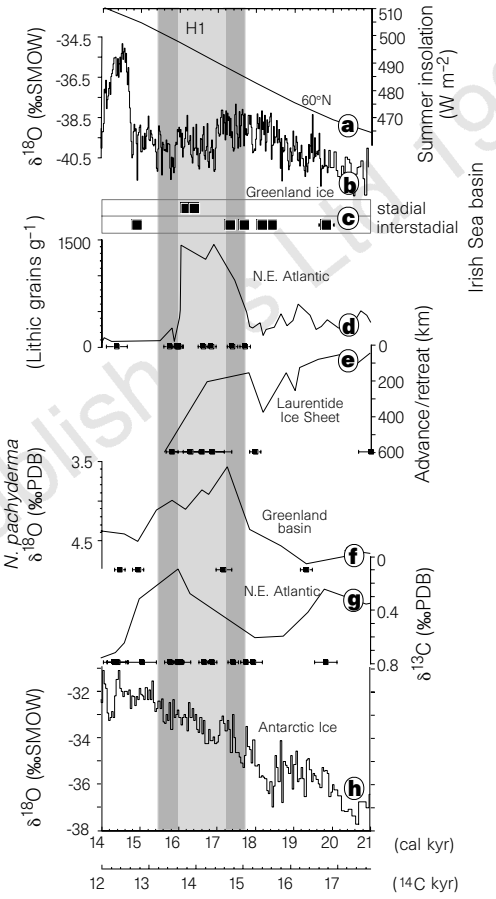

Figure 2 Records spanning the interval from 14–21 calendar kyr (12–17.7 ^{14}C kyr BP, using the calibration of ref. 5) showing varied responses of the climate system at Heinrich event 1 (H1). Uncertainties in the age of the beginning (14.6–15.0 ^{14}C kyr BP) and end (13.2–13.6 ^{14}C kyr BP)[1,4] of H1 are shown by the vertical grey bars. **a**, Insolation values for June at 60° N (in W m^{-2})[27]. **b**, GRIP ice core δ^{18}O record (20-yr means from 14–20 calendar kyr, 50-yr means from 20–21 calendar kyr)[28]. Note that the cooling indicated by the δ^{18}O record (for example, Oldest Dryas) occurred after the beginning of H1 in the GRIP chronology, whereas it occurred at the beginning of H1 in the GISP2 chronology (not shown), a chronology issue. **c**, Radiocarbon ages on our samples from the Irish Sea basin (Table 1) (errors shown where larger than the size of the symbol). Ages constraining glacial advance versus retreat are shown as 'stadial' versus 'interstadial', respectively. **d**, Record of concentration of lithic grains per gram of sediment from North Atlantic core VM23-081 (ref. 1) (54° 2′ N, 16° 8′ W) showing rise in lithic grains during H1. Radiocarbon ages (with errors) constraining the chronology of this record[29] are shown along the base. **e**, Record of advance and retreat (in km) of the Lake Michigan lobe of the LIS[17]. Ice-margin advance is directed up-page; 0 km point is arbitrarily located. Radiocarbon ages (with errors) constraining the age of ice-margin advance during the Crown Point phase[17] are also shown along the base of the record. **f**, δ^{18}O record (in ‰) from core HM94-23 measured on *N. pachyderma* (s.) from the Greenland basin[29] (73° 46′ N, 02° 23′ W). Radiocarbon ages (with errors) constraining the chronology of this record[29] are shown along the base. The large δ^{18}O anomaly (more negative values) reflects the disintegration of the Barents Sea (and possibly the Greenland and Fenno-scandian) ice sheet(s) during H1. **g**, δ^{13}C record (in ‰) *C. wuellerstorfi* from core VM23-81 (ref. 6). Age model is based on radiocarbon ages[6,20] which are shown (with errors) along the base of the record. More negative values of δ^{13}C during H1 indicate a reduction in the strength of NADW. **h**, Byrd, Antarctica, δ^{18}O ice core record (in ‰) (δ^{18}O values from ref. 30; age model of ice core from ref. 21).

Table 1 AMS ^{14}C ages from the Irish Sea basin

Locality/Description/Comments	Laboratory number	δ^{13}C	Radiocarbon age* (yr BP ± 1σ)
Rough Island: Samples from marine mud draping drumlins. Dates marine transgression after ice sheet collapse	AA21822	–2.089	12,740 ± 95
Killard Point: Samples from marine mud interbedded in outwash from the Killard Point moraine. Dates ice sheet readvance	AA22820	–2.607	13,795 ± 115
	AA22821	–2.702	13,955 ± 105
Cranfield Point: Samples from interstadial mud below outwash from the Carlingford Bay ice lobe. Dates ice free interval before readvance	AA21818	–2.097	14,705 ± 130
	AA21819	–1.407	15,605 ± 140
Cooley Point: Samples from interstadial mud below outwash from the Dundalk Bay ice lobe. Records ice free interval before readvance	AA17693	–2.4	15,020 ± 110
	AA17694	–2.5	15,390 ± 110
	AA17695	–2.5	15,400 ± 140
Kilkeel: Samples from interstadial mud below outwash from the Carlingford Bay ice lobe. Dates ice free interval before readvance.	AA22351	–2.019	16,760 ± 130
	AA22352	–2.375	16,750 ± 160

* AMS ^{14}C ages from monospecific samples of *Elphidium clavatum* in marine muds. Samples were submitted to the NSF-AMS facility at the University of Arizona as CO_2. Samples corrected for assumed 400 yr difference between surface-water carbon and atmospheric carbon. Sampling localities shown in Fig. 2.

discharge IRD-laden icebergs between 14.5 and 15.3 ^{14}C kyr BP[18]. Finally, marine-based margins of the Barents Sea and Fennoscandian Ice Sheets (BSIS and FIS) began to retreat 14.7–15.0 ^{14}C kyr BP from their maximum positions which they had maintained since the last glacial maximum (Fig. 2f)[11,19] with icebergs discharged from the retreating margins delivering IRD to the adjacent continental slope and Norwegian Sea[19].

The varied behaviour of amphi-North Atlantic ice sheets during H1 has significant implications for interpreting IRD signals because of the assumed link between ice-sheet advances, which would have delivered IRD to marginal seas, and climate forcing. Comparison of IRD records to the GRIP and GISP2 ice-core records suggests that most Heinrich events and the higher-frequency IRD events occurred at the end of cooling intervals and were followed by abrupt warming (interstadials)[1,20]. Bond and Lotti[1] argued that these events were triggered by climate or a climate-related mechanism because of the relation of the IRD events to cool (stadial) climates, and the fact that more than one ice sheet was involved in discharging icebergs and IRD into the North Atlantic. The record of retreat of the FIS[11] and BSIS[19] during H1 (Fig. 2f), however, indicates that an increase in the flux of IRD-charged icebergs to the open ocean is not necessarily related to a climatically forced ice-margin advance. Insofar as the IRD record of H1 is comparable to deep-sea records of other IRD events, the varied response of amphi-North Atlantic ice margins during H1 suggests the potential for more complex interpretations of other IRD events.

A further implication of our results suggests that H1 is an exception to the common relation between stadial climates and IRD events[20] because it reversed a warming trend clearly seen in Greenland ice-core records (Fig. 2b) and other North Atlantic records[9] that began about 21 calendar kyr BP, when summer insolation at 60° N began to increase (Fig. 2a). Cooling occurred during H1 (for example, Oldest Dryas) as a result of disruption of North Atlantic Deep Water (NADW) formation (and its associated heat transport) by release of meltwater and icebergs (Fig. 2g)[6–8] and continued until the abrupt warming at the onset of the Bølling–Alleröd warm interval. Greenland ice cores suggest that temperatures at the onset of the Bølling–Alleröd reached a level (near interglacial) that was in line with the warming trend started before H1 (Fig. 2b). The warming trend that began in the North Atlantic region about 21 calendar kyr BP also began in Antarctica (Fig. 2h). However, during H1 this warming trend was interrupted in the Northern Hemisphere and as far south as 40° S[5,10], but it continued over most of Antarctica throughout the last deglaciation[21,22] (Fig. 2h). A similar climatic response is associated with discharge of meltwater and icebergs from the LIS during the Younger Dryas[11,12].

In the context of a climate forcing mechanism for Heinrich events[1], the relation of H1 to a warming trend suggests that the cause of H1 may have differed from the cause of the other IRD events[20]. Alternatively, this relation is consistent with a suggestion[23] that Heinrich events originated by an internal instability of the LIS that is independent of climate forcing. This mechanism has been questioned[1] because it does not explain either increased iceberg discharges from multiple ice-sheet sectors and multiple ice sheets, or the increased flux of icebergs from ice streams before discharge along Hudson Strait, as interpreted from the IRD record. However, the example of H1 shows that IRD data in general have the potential for representing a varied and complex response of ice-sheet margins during iceberg-discharge events. Furthermore, lithic data on H1 from deep-sea core VM23-081 (ref. 1) suggest that IRD from various sources, including Hudson Strait, increased at the same time (15 ^{14}C kyr BP). Within the constraints of the radiocarbon chronology, the southern LIS margin was also advancing at this time (Fig. 2e), indicating that much of the LIS margin advanced during H1 (ref. 16). Before H1, the southern LIS margin had been in overall retreat (with secondary, asynchronous oscillations) during the warming trend recorded in Greenland ice cores[16]. This retreat in response to warming is expected, particularly given the extremely low ice-surface gradients that characterized the southern margin[24]. It is unlikely that the observed warming trend before H1 initiated an ice-sheet surge, however, because the effect of such a change in temperature at the ice surface will be strongly attenuated with depth, especially through a thick ice sheet like the LIS[23].

We believe that the timings and patterns of ice-sheet variability in the North Atlantic region discussed here (Fig. 2) are most consistent with the argument that an internal instability of the LIS leading to H1 initiated a sequence of events that were ultimately responsible for reversing initial deglacial warming and thus delaying the transition from full glacial to interglacial conditions at least as far south as 40° S. In particular, discharge of icebergs to the North Atlantic from the LIS would have rapidly reduced formation of NADW[6–8], resulting in cooling of the North Atlantic region[9,25] and causing the Oldest Dryas. The apparent synchronous increase in iceberg discharge from the IIS and LIS[1] may reflect the rapid response of a small ice sheet to this cooling. Alternatively, the example from the BSIS IRD signal[19] suggests that the IIS and GIS[18] IRD signals during H1 may correspond to increased iceberg discharge during retreat of their marine margins. IRD data alone cannot distinguish between these two fundamentally different behaviours. Our evidence for the BIS readvance during H1 is consistent with response of an ice sheet in this climatically sensitive region to North Atlantic cooling. Retreat of the FIS and BSIS margins may also reflect a climatic influence through a reduction of precipitation at these latitudes in association with the cooler North Atlantic region[25]. In addition, their thinned marine margins may have also responded to sea-level forcing associated with the partial collapse of the LIS[26]. □

Received 15 August 1997; accepted 19 January 1998.

1. Bond, G. & Lotti, R. Iceberg discharges into the North Atlantic on millennial time scales during the last glaciation. *Science* **267,** 1005–1010 (1995).
2. Alley, R. B. & MacAyeal, D. R. Ice-rafted debris associated with binge/purge oscillations of the Laurentide ice sheet. *Paleoceanography* **9,** 503–511 (1994).

3. Gwiazda, R. H., Hemming, S. R. & Broecker, W. S. Tracking the sources of icebergs with lead isotopes: the provenance of ice-rafted debris in Heinrich layer 2. *Paleoceanography* **11,** 77–93 (1996).
4. Jennings, A., Tedesco, K. A., Andrews, J. T. & Kirby, M. E. in *Paleoceanography of the North Atlantic Margins* (eds Andrews, J. T., Austin, W. E. N., Bergsten, H. & Jennings, A. E.) 29–49 (Geol. Soc. spec. publ. no. 111, London, 1996).
5. Bard, E., Rostek, F. & Sonzongni, C. Interhemispheric synchroneity of the last deglaciation inferred from alkenone paleothermometry. *Nature* **385,** 707–710 (1997).
6. Jansen, E. & Veum, T. Evidence for two-step deglaciation and its impact on North Atlantic deep-water circulation. *Nature* **343,** 612–616 (1990).
7. Keigwin, L. D., Jones, G. A., Lehman, S. J. & Boyle, E. A. Deglacial meltwater discharge, North Atlantic deep circulation and abrupt climate change. *J. Geophy. Res.* **96,** 16811–16826 (1991).
8. Keigwin, L. D. & Lehman, S. J. Deep circulation change linked to Heinrich event 1 and Younger Dryas in a middepth North Atlantic core. *Paleoceanography* **9,** 185–194 (1994).
9. Bard, E. *et al.* Retreat velocity of the North Atlantic polar front during the last deglaciation determined by ^{14}C accelerator mass spectrometry. *Nature* **328,** 791–794 (1987).
10. Lowell, T. V. *et al.* Interhemispheric correlation of late Pleistocene glacial events. *Science* **269,** 1541–1549 (1995).
11. Lehman, S. J. *et al.* Initiation of Fennoscandian ice-sheet retreat during the last deglaciation. *Nature* **349,** 513–516 (1991).
12. Björck, S. *et al.* Synchronized terrestrial-atmospheric deglacial records around the North Atlantic. *Science* **274,** 1155–1160 (1996).
13. McCabe, A. M. Dating and rhythmicity from the last deglacial cycle in the British Isles. *J. Geol. Soc. Lond.* **153,** 499–502 (1996).
14. Hald, M. *et al.* Recent and Late Quaternary distribution of *Elphidium exclavatum F. clavatum* in Arctic seas. *Cush. Found. Spec. Publ.* **32,** 141–153 (1994).
15. Sissons, J. B. The Loch Lomond Stadial in the British Isles. *Nature* **280,** 199–203 (1979).
16. Clark, P. U. Unstable behaviour of the Laurentide Ice Sheet over deforming sediment and its implications for climate change. *Quat. Res.* **41,** 19–25 (1994).
17. Hansel, A. K. & Johnson, W. H. Fluctuations of the Lake Michigan lobe during the late Wisconsin subepisode. *Sver. Geol. Unders.* **81,81,** 133–144 (1992).
18. Stein, R., Nam, S.-I., Grobe, H. & Hubberten, H. in *Paleoceanography of the North Atlantic Margins* (eds Andrews, J. T., Austin, W. E. N., Bergsten, H. & Jennings, A. E.) 135–151 (Geol. Soc. spec. publ. no. 111, London, 1996).
19. Elverhoi, A. *et al.* The growth and decay of the late Weichselian ice sheet in western Svalbard and adjacent areas based on provenance studies of marine sediments. *Quat. Res.* **44,** 303–316 (1995).
20. Bond, G. *et al.* Correlations between climate records from North Atlantic sediments and Greenland ice. *Nature* **365,** 143–147 (1993).
21. Sowers, T. & Bender, M. Climate records covering the last deglaciation. *Science* **269,** 210–214 (1995).
22. Sucher, C. *et al.* Climate records from the Taylor Dome ice core during the last glacial termination. *Eos* **77,** F429 (1996).
23. MacAyeal, D. R. Growth/purge oscillations of the Laurentide ice sheet as a cause of the North Atlantic's Heinrich events. *Palaeoceanography* **8,** 775–784 (1993).
24. Clark, P. U. Surface form of the southern Laurentide Ice Sheet and its implications to ice sheet dynamics. *Geol. Soc. Am. Bull.* **104,** 595–605 (1992).
25. Fawcett, P. J., Águstsdóttir, A. M., Alley, R. B. & Shuman, C. A. The Younger Dryas termination and North Atlantic Deep Water formation: Insights from climate model simulations and Greenland ice cores. *Paleoceanography* **12,** 23–38 (1997).
26. Locker, S. D., Hine, A. C., Tedesco, L. P. & Shinn, E. A. Magnitude and timing of episodic sea-level rise during the last deglaciation. *Geology* **24,** 827–830 (1996).
27. Berger, A. & Loutre, M. F. Insolation values for the climate of the last 10 million years. *Quat. Sci. Rev.* **10,** 293–317 (1991).
28. Johnsen, S. J. *et al.* Irregular glacial interstadials in a new Greenland ice core. *Nature* **359,** 311–313 (1992).
29. Koç, N. & Jansen, E. Response of the high-latitude northern hemisphere to orbital climate forcing: Evidence from the Nordic Seas. *Geology* **22,** 523–526 (1994).
30. Johnsen, S. J., Dansgaard, W., Clausen, H. B. & Langway, C. C. Oxygen isotope profiles through the Antarctic and Greenland ice sheets. *Nature* **235,** 429–434 (1972).

Acknowledgements. We thank S. Johnsen for the GRIP data, T. Sowers for the Byrd data, D. Bowen and A. Mix for discussion, and R. Alley and J. T. Andrews for reviewing the manuscript. This work was supported by the NSF (P.U.C.).

Correspondence and requests for materials should be addressed to A.M.McC. (e-mail: m.mccabe@ulst.break;ac.uk).

Low-sea-level emplacement of a very large Late Pleistocene 'megaturbidite' in the western Mediterranean Sea

R. G. Rothwell, J. Thomson & G. Kähler

Southampton Oceanography Centre, European Way, Empress Dock, Southampton SO14 3ZH, UK

Large-volume turbidites, termed 'megaturbidites' or 'megabeds'[1], result from catastrophic slope failures and the associated downslope transport of enormous quantities of sediment from continental margins to the deep sea. Such large sediment failures can generate tsunamis[2,3] and, in terrains underlain by gas hydrates (clathrates), may be associated with the release of substantial amounts of the greenhouse gas methane. It has been proposed that the megaturbidite events may be triggered by seismic activity[4], or may result from gas hydrate release itself[5,6], caused by a lowering of hydrostatic pressure on clathrates as a result of low sea level. Previous conclusions on the significance of sea-level change[7–9], however, have been conditional because of the lack of absolute times of turbidite emplacement. Here we use accelerator-mass-spectrometry radiocarbon dating in five widely spaced cores to constrain the date of emplacement of a large-volume (~500 km^3) bed in the Balearic Basin of the western Mediterranean. This turbidite is exceptional in its magnitude and represents the main sedimentation event in the Balearic Basin over the past 100 kyr. Our data provide an estimate of 22,000 calendar years before present for emplacement of the megabed, a time when sea level stood at its lowest level during the Last Glacial Maximum. The coincidence of these dates is consistent with emplacement due to clathrate destabilization caused by low sea level, although other triggering mechanisms, such as seismic shock, cannot be ruled out.

The Balearic Abyssal Plain (Fig. 1) has an area of some 60,000 km^2 and is the largest plain in the Mediterranean Sea. High-resolution 3.5-kHz seismic profiles across the plain consistently show a conspicuous, thick, laterally continuous, acoustically transparent layer (Fig. 2). From such profiles, the layer is estimated to be 8–10 m thick, with its top 10–12 m below the sea floor, just too deep to be recovered fully by conventional piston coring. The layer is of consistent depth and thickness over the entire plain, except at the edges of the basin, where it onlaps the adjacent rise.

Five giant piston cores, 27–36 m in length, were taken ~100–120 km apart on the Balearic Abyssal Plain in 1995 to form an approximately north–south transect in the central plain and an east–west transect in the south of the plain (Fig. 1). The cores were all dominated by sequences of thick structureless muds (commonly grading down to basal sands and silts) separated by foraminifer-rich mud interbeds (generally <20 cm thick). The structureless muds and associated sands and silts are interpreted as turbidites on the basis of their textural characteristics, whereas the foraminifer-rich intervals are interpreted as pelagic accumulation. One particular turbidite mud, conspicuous by its thickness and with a silty to sandy base, was present in all five cores (Fig. 3). The position and thickness of this megabed is similar to that estimated for the acoustically transparent layer. Chemical analysis showed that the megabed mud has a consistent geochemical composition in all five cores, suggest-

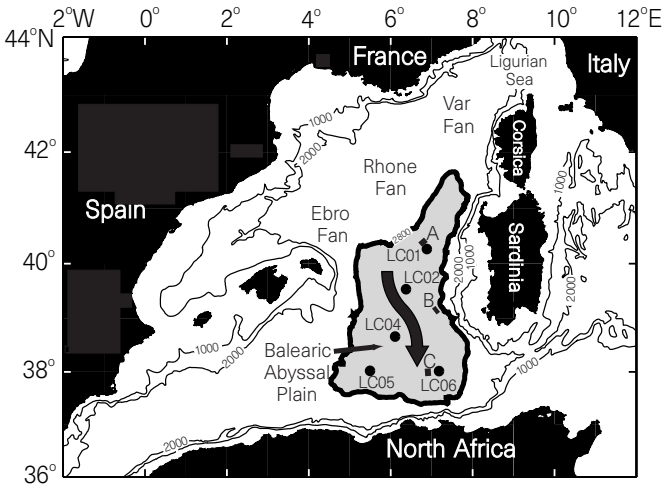

Figure 1 Map showing the positions of the five long piston cores (LC01, LC02, LC04, LC05 and LC06) recovered from the Balearic Abyssal Plain during *Marion Dufresne* cruise 81. The Balearic Abyssal Plain is defined by the 2,800-m contour, shown in bold. The distribution of the megabed is shown by a grey stipple and its emplacement direction by the black arrow. Locations of the 3.5 kHz high-resolution seismic profiles (A, B and C) illustrated in Fig. 2 are also shown. Bathymetric contours are in metres.